Interactions (2025) 246:39
https://doi.org/10.1007/s10751-025-02265-0

CONFERENCE PROCEEDING

Use of deep geothermal energy to supply heat to a village in Scotland

David Penman[1] · Firdaus Muhammad-Sukki[1] · Siti Hawa Abu-Bakar[2] · Nurul Aini Bani[3] · Abdullahi Abubakar Mas'ud[4]

Accepted: 4 February 2025

Abstract

This paper explores the possibility of utilising geothermal energy in an existing district heat network in the Aberdeenshire village of Banchory to provide hot water through the creation of a hypothetical geothermal well. It considers a simulated deep geothermal single well (DGSW), commonly referred to as a coaxial system with a depth of 5000 m. The hypothetical well was created using the dimensions of existing oil wells which, once they have reached the end of their lifecycle, hold the potential to be repurposed for geothermal use. It was found that the thermal output of the well decreases over time due to the drop in local rock temperature which is a result of thermal extraction. Given this, the thermal output after a year of operation was calculated and found that, to directly supply the Banchory heat network, a volumetric flow rate of 4.8m^3/hr was required. After a year of operation, the site's peak thermal production was 108.4 kW which equates to a production of more than 949.9 MWh over the first operational year.

Keywords Geothermal energy · District heat network · Geothermal well · Scotland

✉ Firdaus Muhammad-Sukki
f.muhammadsukki@napier.ac.uk

1 School of Computing, Engineering & the Built Environment, Edinburgh Napier University, Edinburgh EH10 5DT, UK

2 Renewable Energy Research Laboratory, Electrical Engineering Section, British Malaysian Institute, Universiti Kuala Lumpur, Gombak 53100, Malaysia

3 Faculty of Artificial Intelligence, Universiti Teknologi Malaysia, Jalan Sultan Yahya Petra, Kuala Lumpur 54100, Malaysia

4 Department of Electrical Engineering, Jubail Industrial College, Jubail Industrial City 35718, Saudi Arabia

Published online: 12 February 2025

1 Introduction

In 2017 the Scottish government released its energy strategy which included its renewable energy targets for 2030 and 2050. Since the release of this strategy, the Scottish government has remained committed to its renewable aims and achieving net zero by 2050. One of the headline targets introduced was the goal to generate 50% of Scotland's total energy consumption from renewable sources by 2030. Another major goal was to increase Scottish energy productivity by 30% before 2030 [1].

A breakdown of Scottish energy consumption by sector in 2020 is shown in Fig. 1 [2]. The chart shows that heat demand makes up over half of Scottish energy consumption while electrical and transport demand each make up less than a quarter. Scotland's renewable energy generation by major sector from 2009 to 2020 shows that renewable electrical generation has increased by 45.1%, renewable heat generation has increased by 1.9% and the use of renewables in transportation has increased by 2.62% in the last five years. This demonstrates a need for Scotland to shift its focus towards heat consumption and/or renewable transport opportunities if it wishes to meet its 2030 targets.

It is likely that the targets set by the Scottish government will be achieved in ways other than through new renewable projects. With a focus on providing better insulation for homes and a shift to electric vehicles and boilers Scottish energy consumption could soon be dominated by electrical demand. In addition to the targets already discussed the Scottish energy

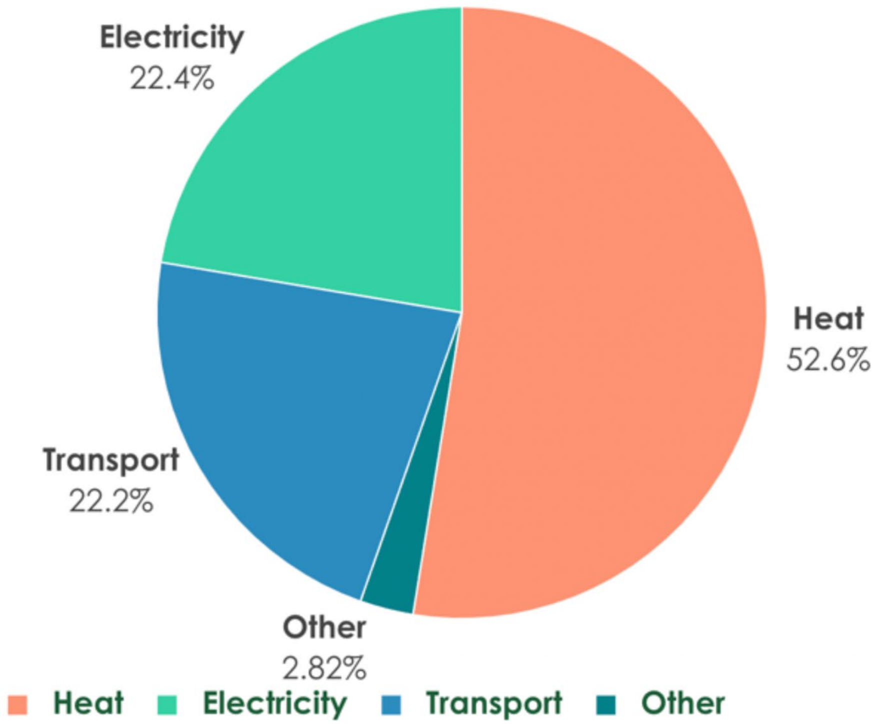

Fig. 1 Total energy consumption by section in Scotland in 2020. Total demand– 146,200 GWh, heat demand– 77,569 GWh (53.1%), Electrical demand– 32,518 GWh (22.2%), transport demand– 32,148 GWh (22%), other– 3,964 GWh (2.71%) [2]

strategy states a desire for a diverse range of renewable sources with a focus on community needs. This represents an opportunity for geothermal power to find its footing in Scotland while its heating systems are being updated for a green future.

Geothermal power can be utilised to heat homes. This can be achieved using district heating to supply heat to multiple buildings or if the demand is high enough a single building. A district heat network is defined as a network in which thermal energy is distributed from one or more sources of production to more than one building [3]. Generally, a network operates by heating water at a central location and pumping it to various homes and/or businesses through a network of insulated underground pipes. The water and space within these premises are heated by this hot water rather than by individual gas or electric boilers. Heat networks allow for a variety of different heating methods including renewables. They can also have higher efficiencies compared to individual boilers assuming that the network has been properly designed and that local heat demand is sufficient. Heat networks can also be referred to as “heat networks” or “district heating”. As of November 2022, heat networks supply 1.5% of Scottish homes [4].

2 The Banchory district heat network

The heat network that the simulated geothermal site will supply lies in the Aberdeenshire village of Banchory. To better understand how heat networks operate the operations of this network will be explained. Banchory is currently home to four heat networks all operated by the same company but only the largest will be discussed. The heat network began operation in 2012 and is currently supplied by two biomass boilers, 700 kW and 900 kW, and two thermal stores of 50,000 L. Additionally, two gas boilers are held in reserve and used to meet peak load demands. The network consists of approximately 6 km of underground piping. The main network pipes are constructed from highly insulated steel with flexible plastic pipes connecting individual buildings to the main steel pipe network. Water leaves the energy centre at a temperature of 80 °C and returns at 60 °C. The centre currently supplies peak heat demand of 7.6 MW and an annual demand of 12,500 MWh [5].

In 2016 the network was examined in a feasibility study that looked at replacing the biomass boilers with a geothermal doublet system to increase the capacity of the network. The location was deemed to have a high enough energy demand to support such a project and to have suitable geothermal properties [6]. Figure 2 shows the existing heat network map in Banchory. It is clear that there is expansion potential for the Banchory heat network.

3 Methodology

In 2016 a geothermal feasibility study of a doublet system was published for the Hill of Fare. Details on the relevant geological specifics are known or have been accurately assumed from data within the report [6]. Additionally, the town is already home to a district heat network, the specifications of which will be used for the creation of this site. Details for the cross-sectional dimensions of the well have been taken from Cheng et al.’s work in examining heat transfer in steam injection wells [7]. The values used are consistent with reports

Fig. 2 Hill of Banchory district heat network map. The red dot showing the location of the biomass energy centre and the yellow dot showing the Banchory sports village [6]

Table 1 Parameters for the simulation geothermal well

Parameters	Value	Unit
Surface temperature	281.15	K
Geothermal gradient	0.0259	°C/m
Depth	5,000	m
Volumetric flow rate	0.000555556	m^3/s
Radius - Inside inner tubing	0.031	m
Radius - Outside inner tubing	0.0365	m
Radius - Inside outer tubing	0.0509	m
Radius - Outside outer tubing	0.0572	m
Radius - Inside casing	0.0807	m
Radius - Outside casing	0.0889	m
Radius - Wellbore	0.1236	m
Density of tubing and casing walls	7,800	kg/m^3
Specific heat capacity of tubing and casing walls	600	J/(kg.K)
Density of cement	2,500	kg/m m^3
Specific heat capacity of cement	1,200	J/(kg.K)
Equivalent absolute roughness	0.00026	m
Thermal conductivity of the insulation	0.027	W/(m.K)
Thermal conductivity of the cement	0.933	W/(m.K)
Thermal conductivity of formation	3.16	W/(m.K)
Thermal diffusity of formation	1.60×10^{-6}	m^2/s
Density of formation	2,650	kg/m^3

published using American onshore oil wells, and the parameters can be found in Table 1 in the results section.

The geothermal well is comprised of two concentric pipes, as shown in Fig. 3. Cool fluid, in this case water, is pumped down the annulus and then back up though the central pipe.

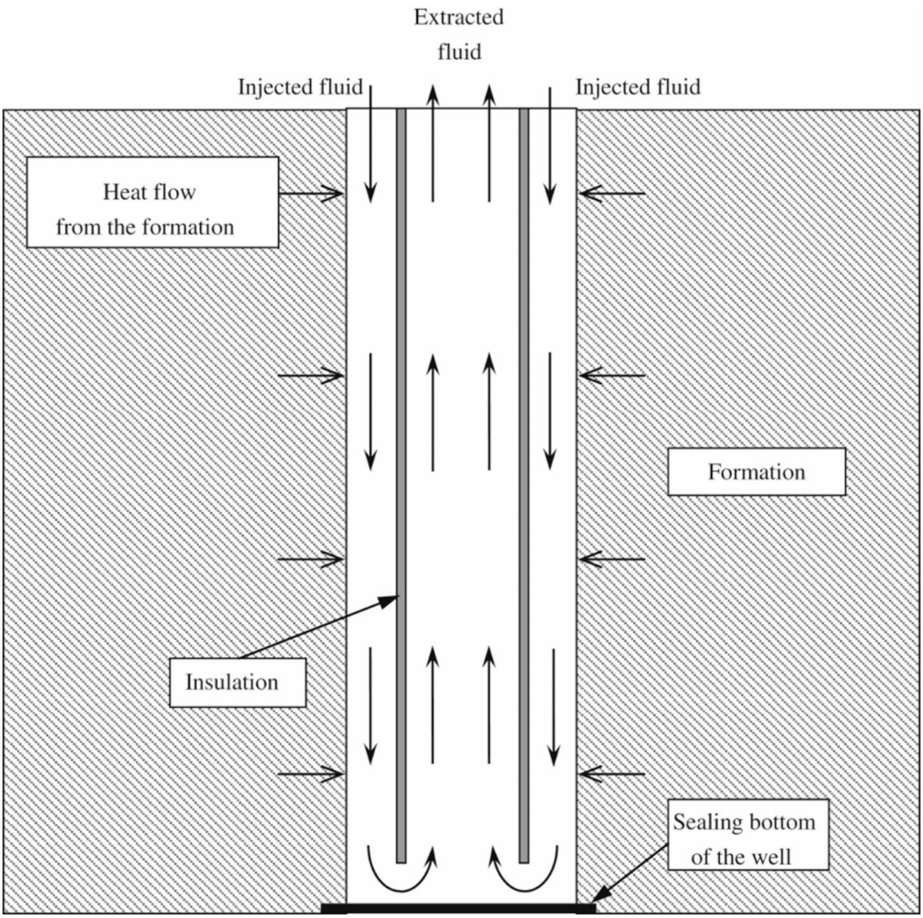

Fig. 3 A structural diagram of the deep geothermal single well. Arrows within the well indicate the direction of fluid flow, arrows within the formation indicate the direction of heat flow after fluid temperature is less than formation temperature [8]

As the fluid travels down the annulus heat transfer takes place between the formation and the fluid.

Figure 4 shows the dimensions of the cross-sectional area of the well. The annulus is bordered by a steel casing which prevents leakage into the formation and a layer of concrete which keeps the well stable. These materials secure the well and provide stability to the system but also act as barriers to heat flow between the well and the formation. Between the inner and outer tubing lies a layer of thermal insulation which prevents heat loss between the extraction fluid and the annulus. Polystyrene was chosen as the insulator for its low thermal conductivity.

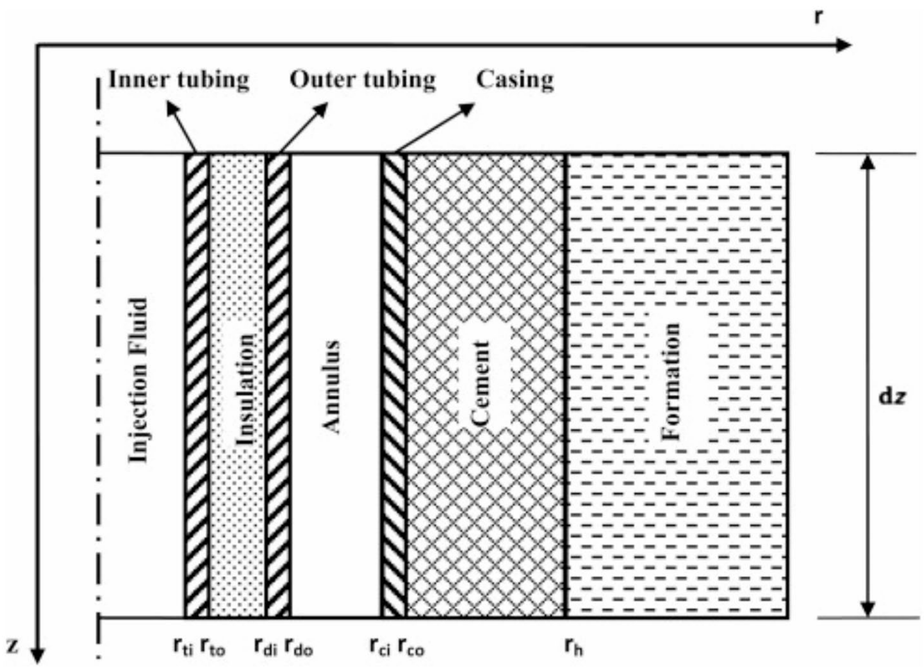

Fig. 4 Schematic of the cross section of the DGSW [7]

3.1 Formation heat transfer model

As fluid is injected into the annulus, heat transfer takes place between the rock formation and the injection fluid. This rate of heat transfer varies with depth, time, and fluid properties but the radial heat flow from the formation can be predicted. Ramey [9] defined the heat flow between the formation and wellbore as follows:

$$\frac{dQ}{dz} = \frac{2\pi\,\lambda_{e}(T_{ei} - T_h)}{f\,(t)} \tag{1}$$

where *dQ/dz* is the rate of heat flow over unit length, W m^{-1}; λ_e is the thermal conductivity of the formation, W m^{-1} K^{-1}; T_{ei} is the formation temperature at an infinite distance from the well axis, K; T_h is the temperature at the edge of the wellbore (marked as r_h on Fig. 4), K; *f(t)* is the transient heat-conduction time function. T_{ei} can be calculated using the following Eq. 2.

$$T_{ei} = T_0 + az \tag{2}$$

where T_0 is the formation surface temperature, K; *a* is the geothermal gradient of the formation, K m^{-1}; *z* is the variable well depth, m.

The transient time function, *f(t)*, has undergone many developments since Ramey's approximate solution in 1962. Equation 3 is an update on the Ramey's solution and factors in the wellbore heat capacity in relation to the formation heat capacity. It should be noted that models for *f(t)* converge as dimensionless time increases [7].

$$f\left(t\right)=\frac{16\omega^{2}}{\pi^{2}}.\int_{0}^{\infty}\frac{1-exp(-\tau_{D}u^{2})}{u^{3}\Delta\left(u,\omega\right)}du \quad (3)$$

where ω is the ratio of the formation heat capacity to wellbore heat capacity, ω= $(\rho C)_e$ / $(\rho C)_h$; τ_D is dimensionless time, as defined in Eq. 4; *u* is a dummy variable for integration; $\Delta\left(u,\omega\right)$ is a function defined in Eq. 5.

$$\tau_{D}=\frac{\alpha_{e}\tau}{{r_{h}}^{2}} \quad (4)$$

where α_e is the thermal diffusivity of the formation, $m^{-2}s^{-1}$; τ is the operational time of the well, s; r_h is the wellbore radius, m.

$$\Delta\left(u,\omega\right)=\left[uJ_{0}\left(u\right)-\omega J_{1}\left(u\right)\right]^{2}+\left[uY_{0}\left(u\right)-\omega Y_{1}\left(u\right)\right]^{2} \quad (5)$$

where J_0 and J_1 are respectively the zero order Bessel function of the first kind and the first-order Bessel function of the first kind. Y_0 and Y_1 are respectively the zero-order Bessel function of the second kind and first-order Bessel function of the second kind.

For long injection times, ${r_h}^2/4\,\alpha_e\tau$ = 1/4 τ_D << 1, this allows Eq. 3 to be simplified to the following Eq. 6. This convergence to take place when τ_D = 20 (this is passed on the third day assuming constant well operation) and so the following expression can be used for long-term analysis.

$$f\left(t\right)=ln\left(2\sqrt{\tau_{D}}\right)-\frac{C_{1}}{2}+\frac{1}{4\tau_{D}}[1+\left(1-\frac{1}{\omega}\right)ln\left(4\tau_{D}\right)+C_{1} \quad (6)$$

where C_1 is Euler's constant, C_1 = 0.5772.

3.1.1 Formation and wellbore heat capacity

As previously stated, the transient time function, *f(t)*, is obtained from the ratio of the formation heat capacity to wellbore heat capacity, *ω*. As we are only interested in the ratio between these two capacities the length of the well can be neglected. The formation heat capacity, $(\rho C)_e$ (J m^{-3} K^{-1}), is defined as the ratio of thermal conductivity to thermal diffusivity in the formation, Eq. 7.

$$\left(\rho C\right)_{e}=\frac{\lambda_{e}}{\alpha_{e}} \quad (7)$$

whereλ_e is the thermal conductivity of the formation, W m^{-1} K^{-1}; α_e is the thermal diffusivity of the formation, m^2 K^{-1}

The thermal conductivity has been estimated from samples using the Hill of Fare data. The thermal diffusivity was not provided in the 2016 feasibility study [6] and so the diffusivity of granite, which comprises much of the formation, has been used [10].

The thermal conductivity of the formation, $(\rho\, C)_h$ (J m^{-3} K^{-1}), can be calculated using Eq. 8. The various radii are labelled in Fig. 4, $(\rho\, C)_{tub}$, $(\rho\, C)_{cas}$ and $(\rho\, C)_{cem}$are the respective volumetric heat capacities for the tubing, casing, and cement of the wellbore. This is found by multiplying the density and the specific heat capacities of the materials used. This assumes the wellbore heat capacity to be the sum of volumetric heat capacities of its components. It also assumes that when compared to the volumetric heat capacities of tubing, casing and cement the volumetric heat capacities of the fluid flowing and insulation are minor and can be ignored.

$$(\rho\, C)_h = \frac{\{\left[\left({r_{to}}^2 - {r_{ti}}^2\right) + \left({r_{do}}^2 - {r_{di}}^2\right)\right] (\rho\, C)_{tub} + \left({r_{co}}^2 - {r_{ci}}^2\right) (\rho\, C)_{cas} + ({r_h}^2 - {r_{co}}^2)(\rho\, C)_{cem}\}}{{r_h}^2} \tag{8}$$

3.1.2 The fluid momentum balance equation

As the fluid flows through the well, its properties change as the temperature and the pressure vary. It is assumed that the fluid flows in a single phase and undergoes no phase transitions. Many models have been developed to accurately describe pressure flow in wells, such as Orkiszewski's method [11] and Beggs and Brill's method [12]. Both of these models describe the flow of two-phase fluid, but they can be adapted for single phase flow. The Beggs and Brill's method has been adopted for this report due to its high accuracy and simplicity to understand. According to the momentum balance principle, the total pressure gradient can be described as follows [12].

$$\frac{dp}{dz} = \rho_{\,f} g sin\,(\theta\,) - \tau_{\,f} - \rho_{\,f} u_f \frac{du_f}{dz} \tag{9}$$

where *dp/dz* is the total pressure change over depth, Pa m^{-1}; $\rho_{\,f}$ is the density of the fluid, kg m^{-3}; g is the force of gravity, m s^{-2}; θ is the well angle from the horizon,°; $\tau_{\,f}$ is the friction-loss gradient, kg s^{-2}; u_f is the velocity of the fluid, m s^{-1}. The well is assumed to be perfectly vertical so θ=-90° for downward flow and θ=90° for upward flow. The fluid velocity can be found using the following Eq. 10.

$$u_f = \frac{V}{A} \tag{10}$$

where V is the volumetric flow rate, m^3 s^{-1}; A is the cross-sectional area, m^2. The cross-sectional areas of the extraction well and annulus can be found by $A_{ext} = \pi\, {r_{ti}}^2$ and $A_{an} = \pi\,({r_{ci}}^2 - {r_{do}}^2)$, respectively.

The fluid properties were initially calculated using the injection pressure and the assumed average temperature in the well. The injection pressure was assumed to be 2 MPa, a value within the range of the following papers [8, 13]. The average temperature was calculated by averaging the fluid flow and return temperatures of the Banchory heat network. After the first model had been built, these properties were updated using the calculated average temperature and pressure for both the annulus and outlet tubes. These properties were manually updated until the average temperature changed by less than 0.1 °C and the average pressure by less than 1 MPa. The properties of the working fluid were collected from the US National Institute of Standards and Technology [14].

The frictional loss gradient is defined as,

$$\tau_f = \frac{f\rho_f {u_f}^2}{2d_h} \tag{11}$$

where f is the friction factor; d_h is the hydraulic diameter of the annulus, which is calculated using Eq. 12, in which P_{an} is the perimeter of the annulus [15]. The hydraulic diameter of the extraction well is simply the pipe diameter.

$$d_h = \frac{4A_{an}}{P_{an}} = \frac{4\pi\left({r_{ci}}^2 - {r_{do}}^2\right)}{2\pi\left(r_{ci} - r_{do}\right)} \tag{12}$$

The friction factor is calculated using Haaland's equation [16]:

$$\frac{1}{\sqrt{f}} = -1.8log_{10}\left[\left(\frac{\Delta/d_h}{3.7}\right)^{1.11} + \frac{6.9}{Re}\right] \tag{13}$$

The Reynolds number and the Prandtl number are calculated using Eqs. 14 and 15, respectively.

$$Re = \frac{\rho_f u_f d_h}{\mu_f} \tag{14}$$

$$Pr = \frac{C_p\mu_f}{\lambda_f} \tag{15}$$

where μ_f is the fluid dynamic viscosity, Pa s; C_p is the fluid specific heat capacity, J kg^{-1} K^{-1}; λ_f is the fluid thermal conductivity, W m^{-1} K^{-1}.

In 1973 Beggs and Brill found that for two phase flow the pressure gradient due to change in kinetic energy, represented by the third term on the right side of Eq. 9, could be rewritten as [12]:

$$\rho_f u_f \frac{du_f}{dz} = -\frac{\rho_m u_m u_{sg}}{p}.\frac{dp}{dz} \tag{16}$$

where ρ_m is the pressure of the liquid gas mixture, kg m^{-3}; u_m is the velocity of the liquid gas mixture, m s^{-1}; u_{sg} is the gas velocity, m s^{-1}; p is the injection pressure. This solution assumes the superficial velocity of the liquid component to be negligible when compared to the superficial velocity of the gas component. It also assumes that the change in the gas mass flux to be negligible compared to the change in gas density. When considering single phase flow the above solution will still be valid if we also assume the change in liquid mass flux to be considerably smaller than the change in fluid density. Therefore Eq. 16 can be rewritten as

$$\rho_f u_f \frac{du_f}{dz} = -\frac{\rho_f {u_f}^2}{p} \cdot \frac{dp}{dz} \tag{17}$$

By combing Eqs. 9, 11 and 17 the pressure depth gradient can be rewritten as

$$\frac{dp}{dz} = \frac{\rho_f g sin(\theta) - \frac{f\rho_f {u_f}^2}{2d_h}}{1 - \rho_f {u_f}^2/p} \tag{18}$$

3.2 The fluid energy equation

The rate of heat transfer between the formation and the wellbore edge, r_h, was described in Eq. 1. The heat transfer is described as unsteady, as the longer the well operates, the greater the effective distance over which the heat transfer occurs. The heat transfer within the well takes place at a set distance and so this heat transfer is described as steady state. Willhite [17] described the rate of heat transfer between the edge of the well and the annulus fluid (for cases in which the fluid is injected into the annulus) as follows.

$$\frac{dQ}{dz} = 2\pi\, r_{ci} U_{ci} \left(T_{an} - T_h\right) \tag{19}$$

where U_{ci} is the heat transfer coefficient based on r_{ci} for elements between the annulus and the edge of the wellbore, W m^{-2} K^{-1}; T_{an} is the temperature of the fluid in the annulus, K.

Willhite's discussion on the heat transfer coefficient predominantly explored cases in which fluid was injected through the central tube (this is the most common configuration for petroleum wells; systems in which fluid travels down the annulus are described as counter flow). By taking Wilhite's overall heat transfer coefficient expression and excluding the materials that don't lie between the annulus fluid and the edge of the wellbore U_{ci} can be found as

$$U_{ci} = \left[\frac{1}{h_c} + \frac{r_{ci} ln\left(\frac{r_{co}}{r_{ci}}\right)}{k_{cas}} + \frac{r_{ci} ln\left(\frac{r_h}{r_{co}}\right)}{k_{cem}}\right]^{-1} \tag{20}$$

where h_c is the convective heat transfer coefficient, W m^{-2} K^{-1}; k_{cas} is the thermal conductivity of the casing, W m^{-1} K^{-1}; k_{cem} is the thermal conductivity of the cement, W m^{-1} K^{-1}. This definition assumes that the heat transfer in the radial direction is dominant over the reverse.

This expression of U_{ci} can be found in the following sources which explore annulus fluid injection in wells [8, 13]. These sources simplify the well cross-section and neglect the thermal resistance of the pipe casing and cement sheath. As the thermal conductivity of the casing is substantially higher than the other materials, it contributes a relatively small portion to U_{ci} and can be ignored. This reduces U_{ci} to the following Eq. 21.

$$U_{ci} = \left[\frac{1}{h_c} + \frac{r_{ci} ln \left(\frac{r_h}{r_{co}} \right)}{k_{cem}} + \right]^{-1} \tag{21}$$

The convective heat transfer coefficient can be calculated as follows for turbulent flow. All flow rates considered in both tubes have Re number in excess of 4000, marking the flows as fully turbulent.

$$h_c = \frac{0.23 \lambda_f Re^{0.8} Pr^{0.4}}{d_h} \tag{22}$$

By combining Eqs. 1 and 18, an expression for the wellbore/formation boundary temperature can be obtained, this is shown below.

$$T_h = \frac{T_{ei} \lambda_e + f(t) r_{ci} U_{ci} T_{an}}{\lambda_e + f(t) r_{ci} U_{ci}} \tag{23}$$

Using the temperature of the fluid injected, the temperature of wellbore edge at depth $z = 0$ can be found. Using Eq. 19, the heat transfer between the annulus and formation edge can be determined and a value for *dQ/dz* found. The rate of heat transfer within each increment of depth is assumed to be constant. The temperature change of annulus fluid can then be calculated using the following Eq.

$$T_{an\,(z+1)} = \frac{\left(\frac{dQ}{dz} \right) \Delta z}{?C_p} + T_{an\,(z)} \tag{24}$$

where Δz is the incremental change in depth (chosen to be 250 m), m; ? is the mass flow rate of the fluid, kg s^{-1}; C_p is the specific heat capacity of the fluid, J kg^{-1} K^{-1}; $T_{an\,(z)}$ is the temperature of the annulus fluid at the begging of the section, K.

The mass flow rate was calculated as shown in Eq. 25.

$$? = V\rho \tag{25}$$

3.3 Counter current fluid heat loss

The heat flow described in Sect. 3.3 is accurate, assuming that there is perfect insulation between the annulus and the extraction well. However, in practice, heat is lost as the fluid travels up the inner pipe. This rate of heat flow is described below [12].

$$\frac{dQ}{dz}_{ext} = 2\pi\, r_{to} U_{to} \left(T_{ex} - T_{an} \right) \tag{26}$$

where dQ/dz_{ext} is the heat flow from the extraction well to the annulus, W m^{-1}; U_{to} is the heat transfer coefficient based on r_{to} for elements between the extraction well and the annulus, W m^{-2} K^{-1}; T_{ex} is the temperature of the fluid in the extraction well, K.

As previously mentioned, Willhite examined the heat transfer for fluid injection into the central tube. There, the radiative heat transfer coefficient for the annulus fluid was included in his expression of U_{to}. As water (a transparent liquid) was chosen as the working fluid radiant heat transfer does not impact the working fluid and U_{to} can be calculated as follows.

$$U_{to} = \left[\frac{r_{to}}{r_{ti}h_f} + \frac{r_{to}\ln\left(\frac{r_{to}}{r_{ti}}\right)}{k_{tub}} + \frac{r_{to}\ln\left(\frac{r_{di}}{r_{to}}\right)}{k_{ins}} + \frac{r_{to}\ln\left(\frac{r_{do}}{r_{di}}\right)}{k_{tub}} + \frac{r_{to}}{r_{do}h_c}\right]^{-1} \tag{27}$$

where h_f is the film heat transfer coefficient for extraction fluid, W m^{-2} K^{-1}; k_{tub} is the thermal conductivity of the tubing, W m^{-1} K^{-1}; k_{ins} is the thermal conductivity of the insulation, W m^{-1} K^{-1}. Since the film heat transfer coefficient of the extraction fluid and the thermal conductivity of the tubing are substantially higher than the other components, they can be excluded, simplifying Eq. 27.

$$U_{to} = \left[\frac{r_{to}ln\left(\frac{r_{di}}{r_{to}}\right)}{k_{ins}} + \frac{r_{to}}{r_{do}h_c}\right]^{-1} \tag{28}$$

Equation 26 can be used to find the rate of heat flow between the extraction well fluid and the annulus fluid. Using this rate of heat flow, the temperature of the extraction well at increment (z– 1) can be determined.

$$T_{ex\,(z-1)} = \frac{\left(\frac{dQ}{dz}\right)\,\Delta z}{?C_p} + T_{ex\,(z)} \tag{29}$$

As the fluid in the outlet has a different average temperature and pressure compared to the annulus, new fluid properties must be determined, which in turn yield a new mass flow rate.

Furthermore, as Eq. 24 only accounts for heat flow from the formation, it must be updated to include the heat flow calculated in Eq. 26. Equation 30 represents the true annulus temperature with respect to depth. This modification creates a loop in the calculations and so the equations must be solved iteratively until convergence.

$$T_{an\,(z+1)} = \frac{\left(\frac{dQ}{dz} + \frac{dQ}{dz}_{ext}\right)\,\Delta z}{?C_p} + T_{an\,(z)} \tag{30}$$

3.4 Site parameters

The parameters of the deep geothermal single well are presented in Table 1. The parameters for the site geology have been taken from the 2016 geothermal energy feasibility study for the Hill of Fare, just outside of Banchory [6]. The well dimensions and material characteristics were taken from a depleted petroleum well in [7]. The dimensions are consistent with other land wells in the United States as confirmed by a directional drilling engineer. The only change from the parameters in [7] was the material used for insulation, which was replaced with polystyrene as used in Davis's 2009 paper [13]. The surface temperature was taken as the yearly average temperature in Banchory, i.e. 8 °C. It is assumed that the fluctuations in this temperature will not have a considerable impact on the overall surface formation temperature.

To directly supply the Banchory heat network a well outlet temperature of 87 °C is required. The heat network currently runs with a departure temperature of 85 °C, and the plate heat exchanger used to connect the two loops requires an outlet temperature of 87 °C. For geothermal projects with district heating applications, it is standard to run two loops of water connected by a heat exchanger, one loop for the well and another for the heat network. In the 2016 Banchory study and the AECC study, a plate heat exchanger was used [18]. In these cases the plate heat exchanger resulted in a 2 °C temperature difference between loops. As the temperature of the return loop of the Banchory heat network is 65 °C this leads to a fluid injection temperature of 67 °C. This results in heat being lost from the inlet flow to the formation until the formation reaches a temperature greater than that of the water. As the water reaches the bottom of the well, it reaches its highest temperature before being pumped up the outlet tube. As the fluid travels up the outlet heat is lost as it flows back to the annulus.

The depth was selected as 5,000 m, the same depth considered in the 2016 Hill of Banchory study. This allows for consistency when using the geological data from the same report. The operational time of the well and the injection pressure rate were initially set at 1 year and 2 MPa respectively. However, after running simulations the injection pressure was changed to 12 MPa to allow for the analysis of a various volumetric flow rates. This pressure lies well within the range of operational parameters for the sample well examined in this paper [19]. The injection pressure has not been optimised for any of the chosen flow rates and could be adjusted to either maximise the heat absorbed by the working fluid or to minimise the pump power demand. After reviewing research by Kujawa et al. [20] on the effects of flow rate on the fluid temperature and heat production of geothermal wells three different volumetric flow rates were tested: 2 m^3/hr, 5 m^3/hr, and 8 m^3/hr.

4 Results and discussions

The following graphs Figs. 5, 6 and 7 show how the water temperature varies with depth for the proposed volumetric flow rates. Each flow rate has been calculated to show the fluid temperature in polystyrene insulation between the annulus and the outlet tube.

When there is no heat transfer between the inlet and outlet tubes a general trend can be found. As the flow rate increases, the outlet temperature decreases. After calculating the thermal power generated, a second trend can be found; as the flow rate increases, so does the power generated, despite the temperature difference between the input and output fluids decreasing.

The graphs show the temperature profile of the well after one year of constant operation. During this year, the local rock temperature around the well will have dropped as thermal energy is gathered and the effective range of heat flow increases. This must be kept in mind when considering the total annual power production of the site. The annual thermal production of each flow rate was found by multiplying the hourly heat generation in a year by the number of hours in the year. This results in a conservative estimate, with the actual thermal generation being much greater.

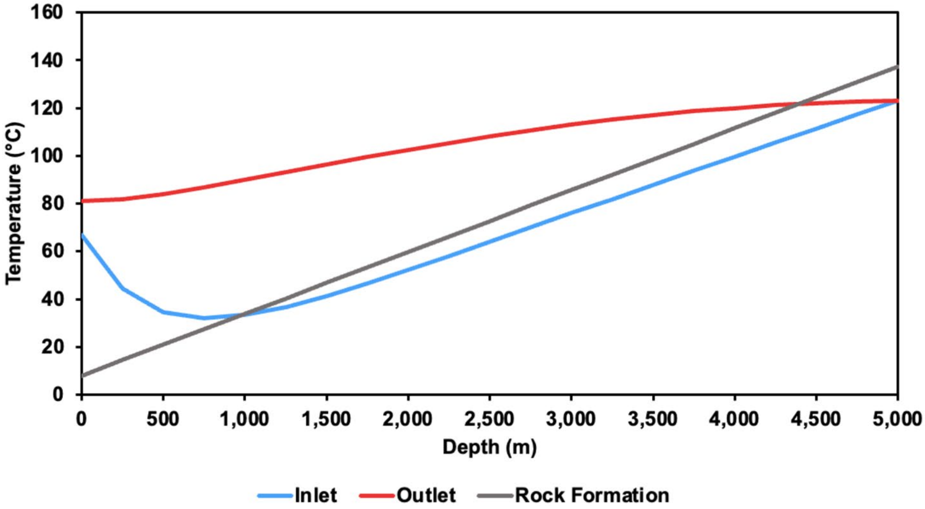

Fig. 5 A graph showing the temperature against depth for the annulus fluid, outlet tube fluid and rock formation. The fluid is injected into the well at a rate of 2 m³/hr and reaches a maximum temperature of 123.1 °C at the bottom of the well with an outlet temperature is 81.1 °C

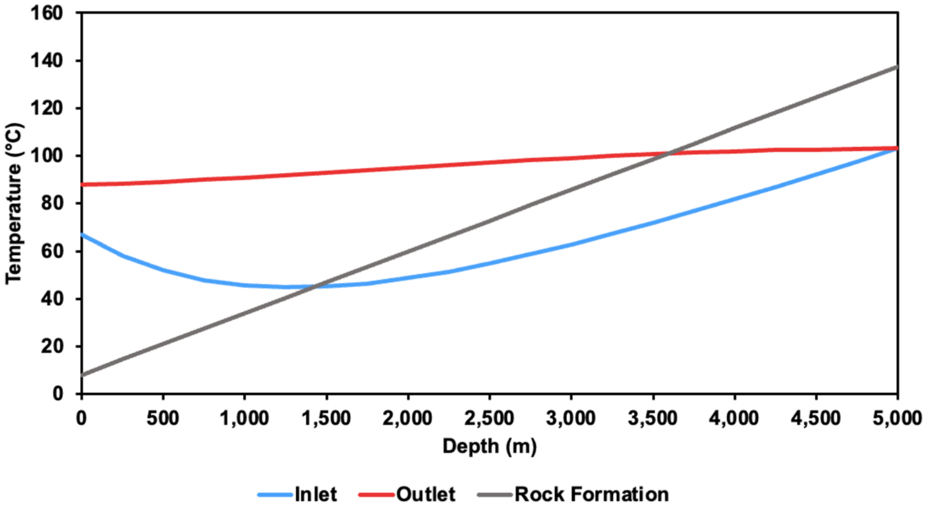

Fig. 6 A graph showing the temperature against depth for the annulus fluid, outlet tube fluid and rock formation. The fluid is injected into the well at a rate of 5 m³/hr and reaches a maximum temperature of 103.1 °C at the bottom of the well with an outlet temperature is 87.9 °C

When considering the various flow rates, V, through the polystyrene insulated well the following can be found.

- For $V = 2$ m³/hr, the outlet water temperature is 81.1 °C and the thermal power obtained is 31.27 kW. This results in an annual thermal production of 277.6 MWh.

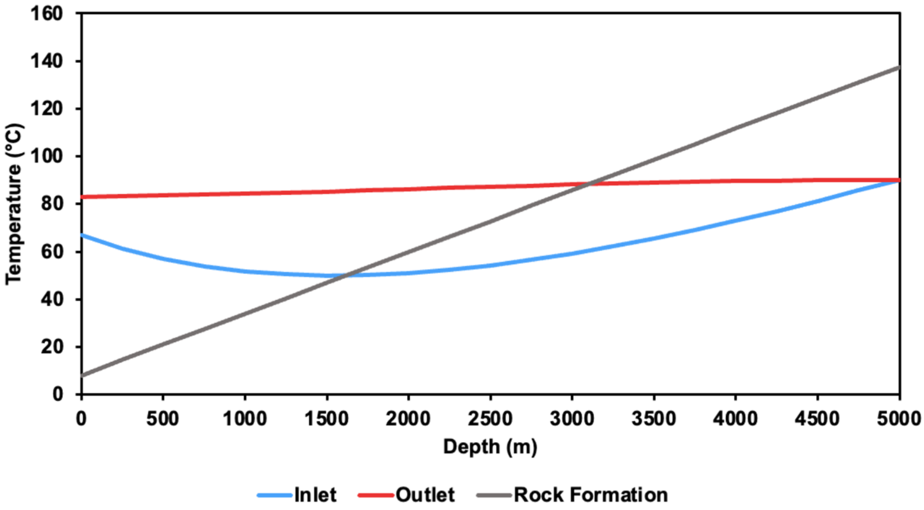

Fig. 7 A graph showing the temperature against depth for the annulus fluid, outlet tube fluid and rock formation. The fluid is injected into the well at a rate of 8 m^3/hr and reaches a maximum temperature of 90.2 °C at the bottom of the well with an outlet temperature is 83 °C

- For $V = 5$ m^3/hr, the outlet water temperature is 87.9 °C and the thermal power obtained is 118.1 kW. This results in an annual thermal production of 1,034.2 MWh.
- For $V = 8$ m^3/hr, the outlet water temperature is 83 °C and the thermal power obtained is 144.6 kW. This results in an annual thermal production of 1,266.8 MWh.

When comparing the graphs of different flow rates in the geothermal well, different trends can be observed. While thermal generation still increases with flow rate, outlet temperature no longer increases as flow rate drops. This results in a maximum outlet temperature somewhere between the flows rates of 2 m^3/hr and 8 m^3/hr. It is possible that as the flow rate continues to increase past 8 m^3/hr, thermal output could drop as the temperature difference between injection and extraction fluids decreases.

The Banchory heat network requires a well extraction temperature of 87 °C. Out of the proposed flow rates, only the 5 m^3/hr could directly supply the network, without requiring a secondary source to heat the water. The 5 m^3/hr flow rate produces an output temperature of 87.9 °C, which is greater than the required temperature. This means that the flow rate can be increased until T_{out} = 87 °C and more thermal energy can be generated for the network. After a secondary analysis, the volumetric flow rate of 5.63 m^3/hr was found to produce the outlet temperature of 87.003 °C and so would be selected to directly supply the network after a year. This flow rate resulted in a thermal output of 127.2 kW and an annual thermal production of 1,114.3 MWh.

5 Conclusions

In this paper, a deep geothermal single well, DGSW, was simulated to supply hot water to the existing district heat network in Banchory. The dimensions of the well were taken from existing oil wells to explore the idea of generating geothermal energy from abandoned oil wells. The model developed considered both the dynamic heat transfer from the formation and heat transfer between the inlet and outlet tubes within the well. The simulation used geological data taken from the Hill of Fare, outside of Banchory, and reached a depth of 5,000 m. Water was chosen as the well's working fluid due to the high operational temperatures in the well and its non-toxic qualities. The district heat network would operate with a departure temperature of 85 °C and a return temperature of 65 °C. Heat from the well would be supplied to the network through a plate heat exchanger, which would result in a well injection temperature of 67 °C and a desired well outlet temperature of 87 °C. The current Banchory heat network is supplied by two biomass boilers, 900 kW and 700 kW, and meets a peak thermal demand of 7.6 MW and an annual demand of 12,500 MWh. After the first year, the system would generate a peak thermal supply of 127.2 kW and which equates to over 1,114.3MWh in the first operational year.

The thermal power generated by this deep geothermal project would not be sufficient to solely supply the Banchory district heat network as it currently operates. This is due to several factors but primarily the required operating temperatures of the heat network. Modern 4th and 5th generation heat networks operate with lower water temperatures. These networks are more common in mainland Europe, but Plymouth is currently considering a 5th generation heat network. A typical 4th generation heat network operates with flow temperatures between 45 °C and 55 °C, while a 5th generation network operates at flow temperatures below 45 °C [21]. Both systems maintain a return temperature between 15 °C and 25 °C [21]. Lower inlet and outlet temperatures would allow higher volumetric flow rates, which would result in a greater thermal yield. Analysis for these temperatures would need to be completed to confirm this assumption.

There are a number of additional variables that could be tweaked to produce greater thermal yields. Working fluids such as isobutane or super critical CO_2 may have better thermal physical properties in these operating conditions and can be considered due to the closed nature of the system. The dimensions of the well and how they effect the pressure differential, which contributes to the pump's power demand, were discussed but not investigated. Changes to the radii of the well interior could produce different fluid pressures and temperatures, which could result in the capture of additional thermal energy.

Acknowledgements The authors would like to thank Edinburgh Napier University for funding the conference.

Author contributions Conceptualization, D.P. and F.M.-S.; methodology, D.P. and F.M.-S.; software, D.P. and F.M.-S.; validation, F.M.-S.; formal analysis, D.P.; investigation, D.P.; resources, D.P. and F.M.-S.; data curation, D.P. and F.M.-S.; visualization, D.P., F.M.-S. and S.H.A.-B.; writing—original draft preparation, D.P.; writing—review and editing, D.P., F.M.-S., S.H.A.-B., N.A.B. and A.A.M.; supervision, F.M.-S.; project administration, F.M.-S.; funding acquisition, F.M.-S. All authors have read and agreed to the published version of the manuscript.

Data availability Data sets generated during the current study are available from the corresponding author on reasonable request.

Declarations

All authors certify that they have no affiliations with or involvement in any organization or entity with any financial interest or non-financial interest in the subject matter or materials discussed in this manuscript.

Competing interests The authors declare no competing interests.

References

1. Scottish Government: The future of energy in Scotland: Scottish energy strategy. Edinburgh, UK 1–89 (2017)
2. Scottish Government: Energy consumption by sector: Whole system. https://scotland.shinyapps.io/Energy/?Section=WholeSystem%26Chart=EnConsumption, last accessed 2024/09/19
3. Scottish Parliament: Heat Networks (Scotland) Act 2021: (2021)
4. Scottish Government: Scotland's Heat Network Fund: Application guidance. https://www.gov.scot/publications/heat-network-fund-application-guidance/, last accessed 2024/09/19
5. HoBESCo Ltd: Our Heat Networks. http://www.hobesco.com/home/about-us/, last accessed 2024/09/19
6. Hill of Banchory Geothermal Energy Consortium: Hill of Banchory Geothermal Energy Project Feasibility Study., Edinburgh, UK: (2016)
7. Cheng, W.L., Huang, Y.H., Lu, D.T., Yin, H.R.: A novel analytical transient heat-conduction time function for heat transfer in steam injection wells considering the wellbore heat capacity. Energy. **36**, 4080–4088 (2011). https://doi.org/10.1016/J.ENERGY.2011.04.039
8. Cheng, W.L., Li, T.T., Nian, Y., Le, Wang, C.L.: Studies on geothermal power generation using abandoned oil wells. Energy. **59**, 248–254 (2013). https://doi.org/10.1016/J.ENERGY.2013.07.008
9. Ramey, H.J.: Wellbore Heat Transmission. J. Petrol. Technol. **14**, 427–435 (1962). https://doi.org/10.2118/96-PA
10. Miranda, M.M., Matos, C.R., Rodrigues, N.V., Pereira, A.J.S.C., Costa, J.J.: Effect of temperature on the thermal conductivity of a granite with high heat production from Central Portugal. J. Iber. Geol. **45**, 147–161 (2019). https://doi.org/10.1007/S41513-018-0096-9/TABLES/6
11. Orkiszewski, J.: Predicting two-phase pressure drops in Vertical Pipe. J. Petrol. Technol. **19**, 829–838 (1967). https://doi.org/10.2118/1546-PA
12. Beggs, H.D., Brill, J.R.: A study of two-phase Flow in inclined pipes. J. Petrol. Technol. **25**, 607–617 (1973). https://doi.org/10.2118/4007-PA
13. Davis, A.P., Michaelides, E.E.: Geothermal power production from abandoned oil wells. Energy. **34**, 866–872 (2009). https://doi.org/10.1016/J.ENERGY.2009.03.017
14. US National Institute of Standards and Technology: Isobaric Properties for Water, https://webbook.nist.gov/cgi/fluid.cgi?ID=C7732185&TUnit=C&PUnit=bar&DUnit=kg%2Fm3&HUnit=kJ%2Fkg&WUnit=m%2Fs&VisUnit=Pa*s&STUnit=N%2Fm&Type=IsoBar&RefState=DEF&Action=Page, last accessed 2024/12/27.
15. Schetz, J.A., Fuhs, A.E.: Fundamentals of Fluid Mechanics. Wiley, Denver, USA (1999)
16. Haaland, S.E.: Simple and explicit formulas for the Friction factor in turbulent Pipe Flow. J. Fluids Eng. **105**, 89–90 (1983). https://doi.org/10.1115/1.3240948
17. Willhite, G.P.: Over-all heat transfer coefficients in Steam and Hot Water Injection Wells. J. Petrol. Technol. **19**, 607–615 (1967). https://doi.org/10.2118/1449-PA
18. Ltd, G.E.: University of St Andrews, ARUP: Deep Geothermal Single Well (DGSW)., Edinburgh,UK (2016)

19. Cheng, W.L., Huang, Y.H., Liu, N., Ma, R.: Estimation of geological formation thermal conductivity by using stochastic approximation method based on well-log temperature data. Energy. **38**, 21–30 (2012). https://doi.org/10.1016/J.ENERGY.2011.12.047
20. Kujawa, T., Nowak, W., Stachel, A.A.: Utilization of existing deep geological wells for acquisitions of geothermal energy. Energy. **31**, 650–664 (2006). https://doi.org/10.1016/J.ENERGY.2005.05.002
21. Jones, P., Dunham, C., Davidson, C.: A roadmap to achieve 5 th generation heat networks in the UK. In: 5th International Conference on Smart Energy Systems. pp. 1–41., Copenhagen, Denmark (2019)